

Estimation of Sea State Parameters from Ship Motion Responses Using Attention-based Neural Networks

Denis Selimović^{a,b}, Franko Hržić^{a,b}, Jasna Prpić-Oršić^a and Jonatan Lerga^{a,b,*}

^aDepartment of Computer Engineering, Faculty of Engineering, University of Rijeka, Vukovarska 58, 51000 Rijeka, Croatia

^bCenter for Artificial Intelligence and Cybersecurity, University of Rijeka, Radmile Matejčić 2, 51000 Rijeka, Croatia

ARTICLE INFO

Keywords:

ship motions
sea state estimation
deep learning
attention neural network
uncertainty estimation

ABSTRACT

On-site estimation of sea state parameters is crucial for ship navigation systems' accuracy, stability, and efficiency. Extensive research has been conducted on model-based estimating methods utilizing only ship motion responses. Model-free approaches based on machine learning (ML) have recently gained popularity, and estimation from time-series of ship motion responses using deep learning (DL) methods has given promising results. Accordingly, in this study, we apply the novel, attention-based neural network (AT-NN) for estimating sea state parameters (wave height, zero-crossing period, and relative wave direction) from raw time-series data of ship pitch, heave, and roll motions. Despite using reduced input data, it has been successfully demonstrated that the proposed approaches by modified state-of-the-art techniques (based on convolutional neural networks (CNN) for regression, multivariate long short-term memory CNN, and sliding puzzle neural network) reduced estimation MSE by 23% and MAE by 16% compared to the original methods. Furthermore, the proposed technique based on AT-NN outperformed all tested methods (original and enhanced), reducing estimation MSE by up to 94% and MAE by up to 70%. Finally, we also proposed a novel approach for interpreting the uncertainty estimation of neural network outputs based on the Monte-Carlo dropout method to enhance the model's trustworthiness.

1. Introduction

Maintaining stable operational performance for ship routing is critical for safety and navigational efficiency. This represents a challenge for onboard decision support systems (DSSs), which consider the problem of obtaining data on the surrounding sea state and help make operational decisions more precise Faltinsen (1990). Since encountered waves affect almost all ship operations, real-time estimation of their characteristics is of crucial importance. Different approaches for collecting information about sea state data exist. Moored wave buoys, navigational radars, or satellite data are traditionally used. However, these methods do not represent a complete solution due to their limitations in availability, reliability, convenience and/or cost of maintenance Nielsen (2017). For example, statistical-based methods can provide accurate wave height estimates, but wave period and wave direction estimates are relatively poor. On the other hand, expensive wave radars can produce accurate estimations of wave period and wave direction, but wave height is not always estimated correctly Selimović, Lerga, Prpić-Oršić and Kenji (2020).

As a more efficient alternative to standard estimation methods, the concept of a "wave buoy analogy" intends to measure only available ship responses to infer sea state information. These result in less complexity, easier maintenance, and ultimately lower costs. Decades of research have been

conducted on this concept. A concise overview of sea state estimation techniques based on ship motions is given in Nielsen (2017). Optimization methods were developed and refined as computing resources improved. Ultimately, this results in several published research papers incorporating the speed-of-advanced problem and full-scale tests. The concept is introduced with the assumption of linearity between sea state and measured ship responses. With an appropriate mathematical model, two different estimation approaches can be found in the literature, one in the frequency domain and another directly in the time domain. The latter intends to address challenges that appear in frequency domain procedures. In the time domain, research focuses on methods that apply Kalman filtering Pascoal and Guedes Soares (2009); Pascoal, Perera and Guedes Soares (2017) or step-wise procedures Nielsen, Bjerregård, Galeazzi and Fossen (2015); Nielsen, Galeazzi and Brodtkorb (2016). However, most of the research done in the frequency domain uses spectral analysis, with a mathematical relationship between the response spectra and the directional wave spectrum (DWS). The model description is given with complex transfer functions, i.e., response amplitude operators (RAOs). The corresponding DWS is then found by inverse mapping procedures. Procedures in the frequency domain are formulated so that the mathematical model is based either on the equivalence of spectral energy distribution Nielsen (2006); Tannuri, Sparano, Simos and Da Cruz (2003); Hinostroza and Guedes Soares (2016) or the spectral moments Montazeri, Nielsen and Juncher Jensen (2016).

Although the above-mentioned DWS estimation techniques have shown fine performance in many reports, their implementation may include some constraints. The concept of analogy is given with the assumption of linearity, and

*Corresponding author

✉ dselimovic@riteh.hr (D. Selimović); fhrzic@riteh.hr (F. Hržić);
jasnapo@riteh.hr (J. Prpić-Oršić); jlerga@riteh.hr (J. Lerga)
ORCID(s): 0000-0003-2485-0416 (D. Selimović); 0000-0003-2485-0416
(F. Hržić); 0000-0002-5742-6067 (J. Prpić-Oršić); 0000-0002-4058-8449 (J.
Lerga)

spectral analysis requires stable operating conditions where it should be a certain minimum period of stationarity to perform one. In addition, the accuracy and reliability of estimation largely depend on the accuracy of RAOs which may be less accurate or incomplete due to insufficient knowledge of the input conditions. Recently, sea state estimation was related to data-driven ML approaches to overcome the limits of conventional RAO-based methods. The idea is to build a parametrized ML model without knowledge about ship model description. A few studies have been published on the use of ML approaches to train the model. The proposed models, trained on time and/or frequency domain features, have shown sufficient accuracy in predicting wave characteristics. As the model is based only on ship motion data, the assumption is that it can be adapted to various types of ships. An example of a model-free approach to identify sea state levels is proposed by Tu, Ge, Choo and Hang (2018). The authors apply available dynamic positioning (DP) sensors to collect time-series data in four degrees of freedom (DOF). The estimation procedure includes multi-layer classifiers, and time and frequency domain features are extracted from the data with several preprocessing techniques.

As the classification in feature-based approaches is dependent on the quality and quantity of hand-engineered features, research suggested the application of DL methods. The DL-based model for classifying the sea state levels proposed by Cheng, Li, Skulstad, Chen, Hildre and Zhang (2019) uses only raw time-series data. Here, the classification accuracy is improved using a multi-component model. Namely, convolutional neural networks (CNNs) and fast Fourier transform help extract time and frequency characteristics, while recurrent neural networks search for long dependencies in motion data. Cheng, Li, Ellefsen, Chen, Hildre and Zhang (2020a) expanded this work using densely connected CNN to take into account the estimation of wave direction characteristics. Additionally, to improve the interpretability and achieve even better accuracy, Cheng, Li, Skulstad, Zhang and Chen (2020b) proposed a model based on 2D spectrogram images, which carry both time and frequency information.

The before-mentioned papers are related to DP application without ship forward-speed. On the other hand, Duz, Mak, Hageman and Grasso (2019) and Mak and Düz (2019) successfully predicted wave height and wave direction under forward-speed conditions. Ship motions in 6-DOF are used as input, and the problem was treated as a multivariate time-series regression. Results are given for several NN structures with appropriate performance comparisons. Those works are extended to identify real-time DWS using deep convolutional encoding-decoding NN in Scholcz and Mak (2020). However, the approach is focused on training models on simulated data, and then these models are used for measured data directly or applied using transfer learning methods. In Mittendorf, Nielsen and Bingham (2022) several proposed DL architectures also prove sufficient results in the case of an advanced ship in beam and following seas with no significant effect on the prediction accuracy when a different forward-speed is applied.

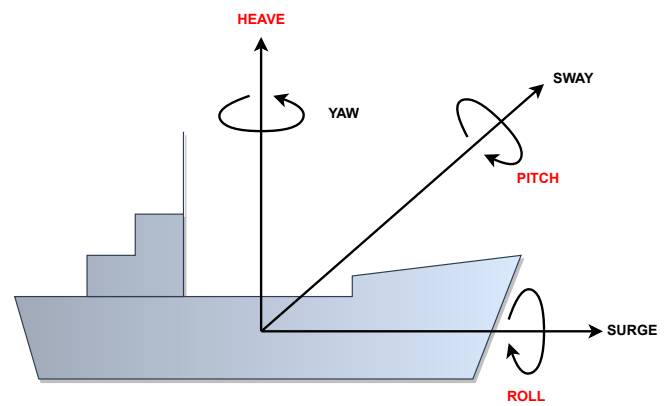


Figure 1: Ship motion responses in six degrees of freedom (6-DOF).

In this paper, we propose several DL models for sea state parameter estimation. The main focus was on improving the currently proposed models and implementing the new DL model based on AT-NN. The input data was 3-DOF ship motion time-series, and the output indicated the wave period, relative wave direction and significant wave height. As in Duz et al. (2019), the problem was characterized as a multivariate time-series regression. The algorithms are trained with numerically simulated data generated according to the recommended guidelines. Proposed methods have been compared to state-of-the-art reports to evaluate the novelty of the research and its potential real-life applications.

The rest of the paper is structured as follows. In Section 2, the data generation process is given with described simulation procedure. Next, the applied NN architectures and DL models are described. The performances of applied models were evaluated and described in Section 3. Conclusion remarks on the limitations of the present work and possible future works are provided in Section 4.

2. Methods

Collecting real-time estimation of encountered wave characteristics may be worthwhile for improving navigational efficiency. While routing, the ship encounters stochastic environmental forces, thus subjected to three rotational (rolling, pitching, and yawing) and three linear (surging, swaying, and heaving) motion responses, as shown in Figure 1. According to many previous studies mentioned in the introduction of the paper, considering a set of three motion responses is advantageous for successful sea state estimation in a wave buoy analogy approach. Based on the given input-output data pairs, the idea is to create a DL model to estimate the characteristics of encounter waves with given ship motion responses in 3-DOF. We observe the roll, pitch, and heave motions, mostly driven by the sea waves and least affected by the operation of the thrusters Selimović et al. (2020); Nielsen (2006).

For testing DL model accuracy, stationary stochastic time-series of 3-DOF ship motion responses are computed from the known wave spectra. Time-series simulation procedures are done according to recommended guidelines given in DNV-GL (2018), and related research work by Mittendorf et al. (2022). This section describes the used procedures for generating time-series data and models for wave characteristics estimation.

2.1. Computing of time-series data

Let us suppose the ship is navigating in the natural seaway, i.e. in irregular waves, at a specified forward speed, U , and with a relative heading to the waves, β . In this case wave elevation can be expressed as a sum of multiple sinusoidal (regular) wave components:

$$\zeta(x, t) = \sum_{i=1}^n A_i \cos(\omega_i t - k_i x + \epsilon_i) \quad (1)$$

where ω_i is a wave frequency of a particular wave component, k_i is a wave number, and ϵ_i is a the random phase shift in the range $[0, 2\pi]$ to ensure random nature of the waves. The amplitude A_i can be found from the relation to the wave spectrum $S(\omega)$, given with equation 2:

$$\frac{1}{2} A_i^2 = S(\omega_i) \Delta\omega_i \quad (2)$$

where considered frequency interval $\Delta\omega_i$ has randomly distributed boundaries.

Wave spectrum $S(\omega)$ is given in the frequency domain and describes how the total wave energy of all wave frequencies ω_i is distributed in stationary seaway Faltinsen (1990). It can be estimated by one of the well-known equations suggested by the International Towing Tank Conference ITTC (1969). In the case of fully developed seas, the recommendation is to use the two-parameter Bretschneider spectrum, cf. Eq. 3.

$$S(\omega) = 124 \frac{H_s^2}{T_z^4} \omega^{-5} \exp\left(-\frac{496}{T_z^4 \omega^4}\right) \quad (3)$$

The equation 3 is given in a rewritten form as the characteristic statistical period of interest is zero up-crossing period T_z , with a relation to mean wave period T_1 , $T_1 = 1.087 T_z$ and peak period T_p , $T_p = 1.405 T_z$. H_s represents significant wave height, and ω is the wave frequency DNV-GL (2018).

The energy distribution, in an example of two-parameter Bretschneider spectrum, is given in Figure 2 with values of $H_s = 3.0$ m and $T_z = 4.0$ s. The one-dimensional spectrum has a single peak value indicating that unimodal seas are being observed. The single peak value occurs at an angular frequency $\omega_p = 1.12$ rad/s, corresponding to the above relations for the peak period T_p and zero up-crossing period T_z since $\omega_p = 2\pi/T_p$. Also, the supplied spectrum includes

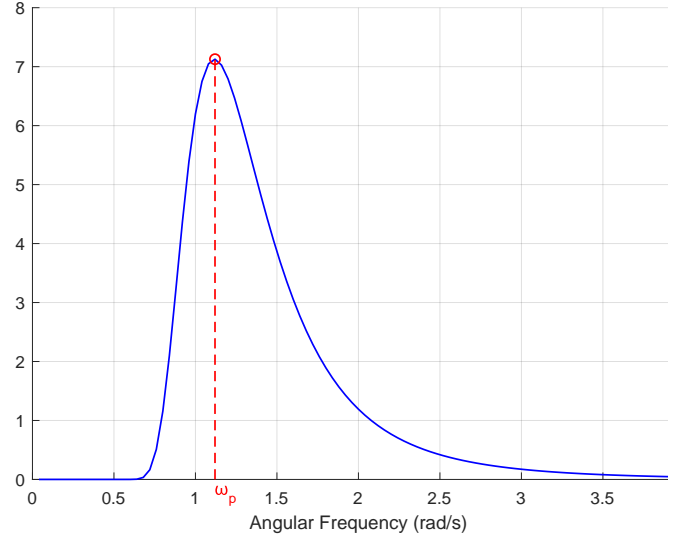


Figure 2: Unidirectional one-dimensional Bretschneider wave spectrum with $H_s = 3.0$ m and $T_z = 4.0$ s.

information on the significant wave height H_s , which can be determined from the area under the spectrum. It should be noted that, for practicality and simplicity reasons, generated time-series do not contain information about wave directionality. In other words, we only observe long-crested or unidirectional waves with a narrow spreading.

While routing, the ship is observed as a complex object with the forward speed U , and it is encountered by waves at a specific encounter angle β . Encountered wave spectrum is not equal to wave spectrum given in wave frequency domain ω due to Doppler shift. Therefore, ship responses should be observed in the encounter frequency domain ω_e . The following expression applies to the transformation from wave to encounter frequency domain:

$$\omega_e = \omega - \frac{\omega^2 U}{g} \cos(\beta) \quad (4)$$

with g being the gravitational constant in the adopted right-handed coordinate system, where the encounter angle of $180deg$ indicates head seas.

With known encounter wave spectrum and appropriate complex-valued transfer functions Φ_R , one can calculate the time-series of ship motion responses $R_i(t)$ following Denis and Pierson (1953):

$$R_i(t) = \sum_{i=1}^n A_i |\Phi_R(\omega_{e,i})| \cos(\omega_{e,i} t + \epsilon_i) \quad (5)$$

where frequency discretisation is non-equidistant, and amplitude A_i is given in wave frequency domain ω as stated in Eq. 2. Since the unidirectional spectrum is observed, each set of time-series $R_i(t)$ is generated for a single encounter angle β , with other wave characteristics contained in the amplitude A_i .

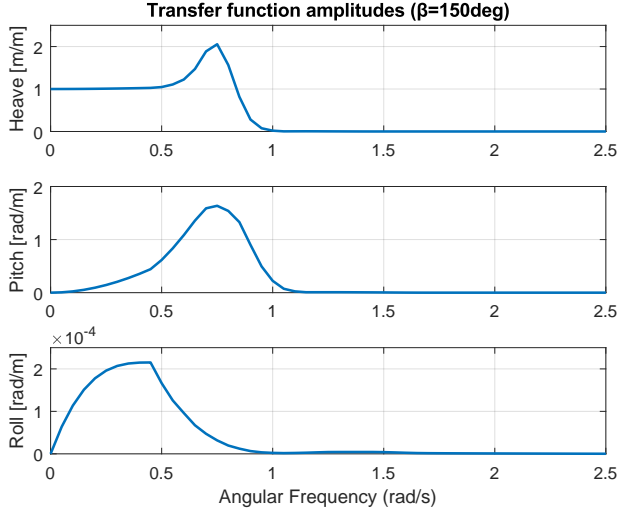


Figure 3: Amplitudes of transfer functions for heave, pitch and roll responses with relative wave direction $\beta = 150$ deg. and ship forward speed $U = 16.19$ knots.

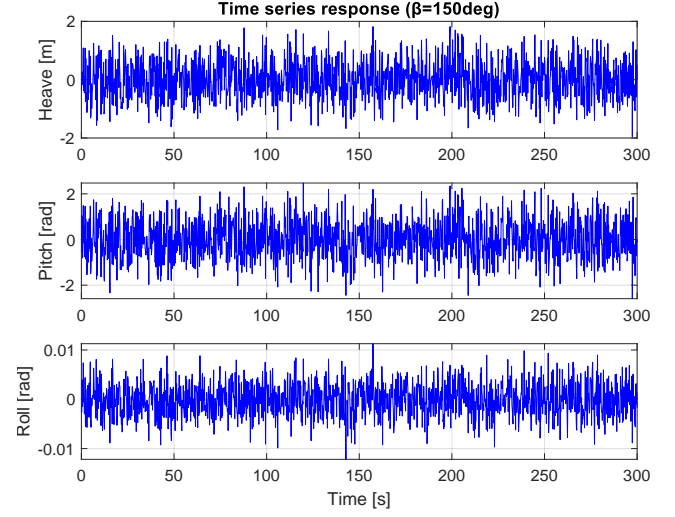


Figure 4: Calculated time-series of ship motion responses at ship forward speed $U = 16.19$ knots and sea state parameters $H_s = 3.0$ m, $T_z = 4.0$ m and $\beta = 150$ deg.

Table 1

Main characteristics of the Bulk Carrier ship.

Name	Value
Length L_{PP}	160.4 m
Breadth B	27.2 m
Draught T	6.55 m
Metacentric height G_M	3.97 m
Block coefficient C_B	0.77
Displacement	22,193 t

Transfer functions are computed with a strip theory solver for pitch, roll and heave as a function of encounter frequency ω_e and encounter angle β . Forward speed was 16.19 knots, and relative wave directions were discretized into 36 headings for $[0, 360]$ deg, with other values obtained by linear interpolation. The range of wave frequencies ω are defined as $[0, 4.0]$ rad/s. The ship under study was a 20,000DWT Bulk Carrier, with the primary characteristics shown in Table 1. The amplitudes of frequency response functions for heave, pitch, and roll motions are given in Figure 3 with relative wave direction $\beta = 150$ deg and ship forward speed $U = 16.19$ knots.

By applying the Eq. 5, we computed time-series of motion responses in 3-DOF, with a sampling frequency of 5 Hz and sample lengths of 300 s. An example of time-series responses is given in Figure 4. We design Latin hypercube sampling (LHS) to discretize the three-dimensional search space of H_s , T_z and β with a 20,000 number of sample points at a uniform distance. The range of validity for parameter H_s is $[0.5, 10.5]$ m and $[3.5, 9.6]$ m for parameter T_z . The encounter angle β is defined in range $[0, 360]$ deg. In addition, following Mittendorf et al. (2022) work, constraints for irregular waves are applied to include wave

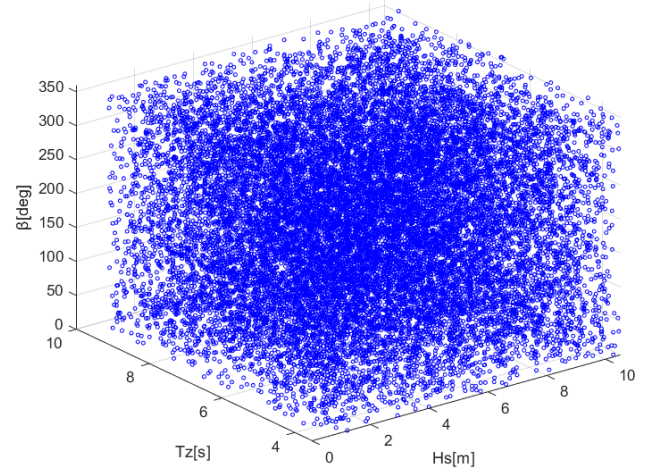


Figure 5: Wave spectra parameters H_s , T_z and β uniformly distributed using Latin Hypercube Sampler.

breaking conditions in the sense of moderate wave steepness with a limited maximum value S_s given as DNV-GL (2018):

$$S_s = \begin{cases} \frac{1}{10} & \text{for } T_z \leq 6 \text{ s} \\ \frac{1}{15} & \text{for } T_z \geq 12 \text{ s} \end{cases} \quad (6)$$

Finding the values between the limits given in the above equation is done with linear interpolation. The dataset contained about 13,000 samples after these constraints were applied. The final three dimensional search space of H_s , T_z and β designed by LHS is presented in Figure 5. The following is a detailed description of the data augmentation process and the NN architectures which are used to create the DL models.

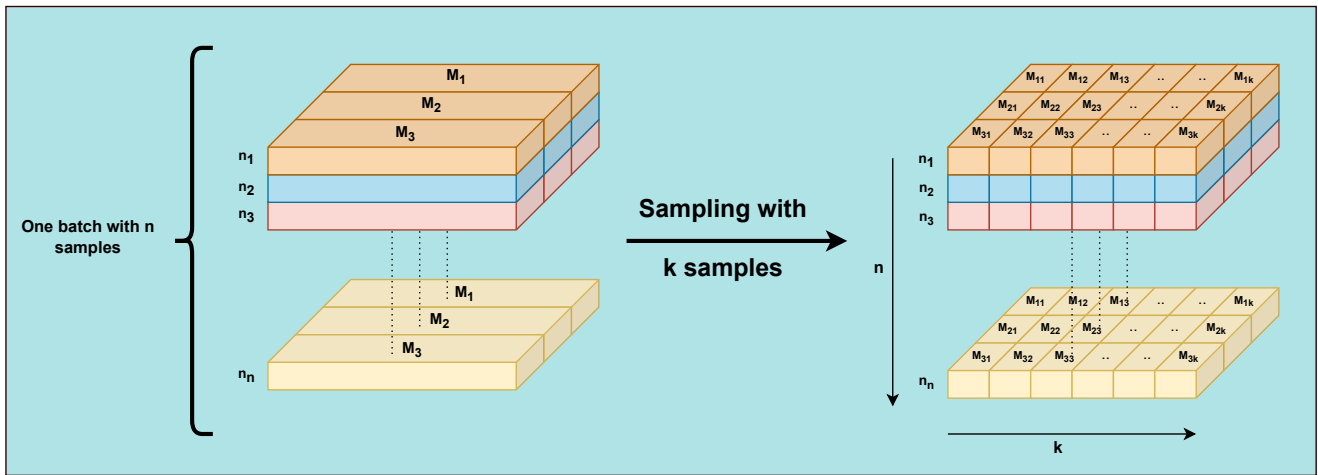


Figure 6: Data augmentation modelling with more samples.

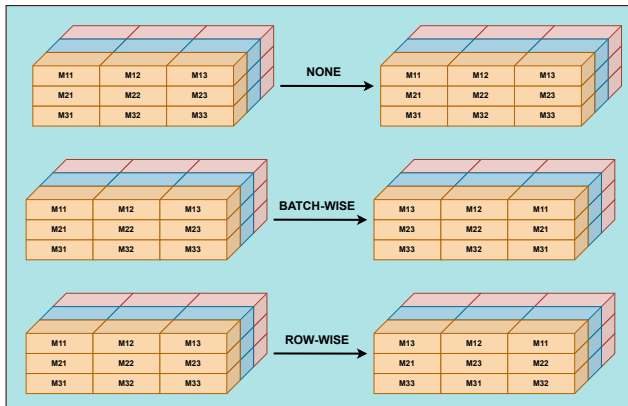


Figure 7: Comparison of batch-wise and row-wise data augmentation.

2.2. Data preprocessing

Input-output samples were prepared for models' training in the form of JSON files, and subsequently processed and scaled. The output values of the sea state parameters were scaled so that H_s and T_z were divided by a value of 15, and the relative wave direction β values were divided by the value of 360. The extensive experimentation showed that the scaling of input data (3-DOF) is not influencing the convergence of the tested models. However, the convergence of models is greatly influenced by the output scale (set to be between 0 and 1). By choosing scaling values of 15 and 360 as maximum values in our dataset enlarged by 10%, we have ensured the fulfillment of these conditions.

Data augmentation strategies are employed in the data preprocessing step to increase the accuracy of our models. With data augmentation applied to proposed models, we increase the variety of our data and eliminate overfitting.

Next, we explain the utilized data augmentation methods. Figure 6 shows one batch with $n = 32$ samples. Each sample in the batch consists of three time-series input data of ship motion responses, denoted as M_1 , M_2 and M_3 .

Within each batch, sampling with size $s = 32$ was performed resulting in $k = 47$ sub-samples of each input data.

Figure 7 compares transformations on how the sub-samples of each input data are shuffled. We distinguish two different approaches: batch-wise and row-wise types of augmentation. Comparison is given using one batch with $n = 3$ samples and $k = 3$ tokens. As depicted in the figure, batch-wise augmentation randomly shuffles the input data signals so that all rows shuffle simultaneously in the same manner. Row-wise augmentation, on the other hand, shuffles each data sample separately. To compare the results, all DL models were trained without any augmentation, as well as with batch-wise and row-wise data augmentation. The trained models always outperformed those not using the above data augmentations.

2.3. Deep learning models

In this research, we propose a novel DL model for sea state parameter estimation based on the current state-of-the-art module called Attention Vaswani, Shazeer, Parmar, Uszkoreit, Jones, Gomez, Kaiser and Polosukhin (2017). To prove that the proposed model is fine-tuned and can be treated as the best currently available solution, we have compared it with the three other DL models presented in Mak and Düz (2019). Furthermore, to correctly compare the proposed model with existing models, we have enhanced the existing models by scaling the number of kernels and neurons. Here we find the work done by Mak and Düz (2019) to be the most relevant due to several facts: their approach is well defined and enables their models' reproductivity, proposed models are based on different modules, and last but not least, they have been dealing with the same problem as the one addressed in this paper. The only difference between our utilization of existing models and their original usage was the number of input signals. Namely, in the original paper, the existing models utilized 6-DOF of ship motion, while our experiments only used 3-DOF. By reducing the number of DOF, we did not impair the model's integrity in

any way, which is supported by the obtained results which are comparable to the results in the original paper.

In the following subsections, the utilized DL models will be presented and described in detail, while the source code implementing the models can be found in the following repository Selimović, Hržić, Prpić-Oršić and Lerga (2022). Furthermore, at the end of this subsection, we provide a short summary of all models' hyperparameters.

2.3.1. CNN for regression: original and enhanced

The first NN presented in Mak and Düz (2019) was the most straightforward NN based on convolutions. Hence, CNN-REG perfectly fits this DL model: a CNN for regression. The NN consisted of two convolutions and a dense layer mainly followed by the *tanh* activation functions (as depicted in Figure 8). The first convolutional layer had 48 filters with kernel size 3×15 , while the second convolution layer had 48 filters with kernel size 1×9 . The dense layer consisted of 30 neurons followed by the dropout layer with the dropout probability set to 0.25. Furthermore, we have experimented with the values of the following hyperparameters to find the best possible performance:

- max pooling kernel sizes: 1, 3, 5, 7, 10,
- scaling factor κ : 1, 5, 10,
- Tested optimizers were *ADAM* and *SGD* both with learning rates $\alpha = 5 \cdot 10^{-3}, 5 \cdot 10^{-4}, 5 \cdot 10^{-5}$,
- Data augmentation: *row-wise* and *batch-wise*.

Let us note that the NNs proposed by Mak et al. were enhanced by adding a scaling factor that increases the "width" of the NN. The width is enhanced by multiplying the number of filters in convolutional layers and the number of neurons in dense layers by scaling factor κ . For example, the initially proposed number of filters in the first convolutional layer was 48, which after the scaling by $\kappa = 5$, becomes 240. This way, we did not just compare our proposed AT-NN DL model with current state-of-the-art NNs; we have even tried to enhance the originally proposed models. Therefore we will present results for two versions of the CNN-REG NN topology: the original one (*CNN-REG-ORG*) and the enhanced one (*CNN-REG-ENH*).

The parameters for *CNN-REG-ORG* are same as stated in Mak and Düz (2019) ($\kappa = 1$, max pooling kernel size equal to 3) except we have used *SGD* with learning rate $\alpha = 0.005$ since the originally proposed learning rate $\alpha = 0.03$ would not converge on our dataset. As best dataset augmentation for this model was shown to be "Row-wise" data augmentation. For the *CNN-REG-ENH* the best performing parameters were as follows: $\kappa = 10$, max pooling kernel size 5, optimizer *ADAM* with learning rate $\alpha = 0.0005$, and data augmentation *row-wise*.

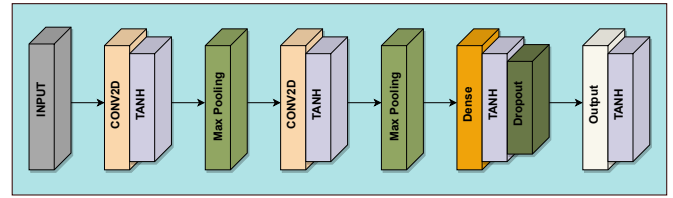


Figure 8: The architecture of the convolutional neural network for regression (CNN-REG).

2.3.2. Multivariate long short-term memory CNN (MLSTM-CNN): original and enhanced

Multivariate long short-term memory (LSTM) CNN consists of two components, as depicted in Figure 9. The first component is based on convolutions (similar to the CNN-REG model) but enhanced with squeeze and excitation block (SEB) Hu, Shen and Sun (2018). SEB block introduces weights that increase inter-dependencies among the convolution layers feature maps while simultaneously adding minor computational costs. The second component is based on the LSTM block Hochreiter and Schmidhuber (1997). The LSTM block introduces memory that is able to "remember" the dependencies between the signal sample in the observed moment and all samples before the observed moment. The multivariate long short-term memory convolutional neural network (MLSTM-CNN) is built the same way as proposed in Mak and Düz (2019): the first convolution layer had 16 filters with kernel size 3×11 , while the second and third convolution layer had 32 filters with a kernel size of 1×6 and 1×3 respectively. The LSTM layer had depth 8 (number of LSTM blocks stacked one on top another) each with 32 neurons (filters), and SEB block utilized "shrink" ratio of $r = 16$. Finally, the dense layer consisted of 8 neurons. This setup we have called *MLSTM-CNN-ORG*. Next, by multiplying each number of neurons/filters by a factor κ , we created an enhanced version named *MLSTM-CNN-ENH*.

The tested hyperparameters for MSLSTM-CNN are related to scaler value κ chosen among the following options: 1, 5, and 10. Other hyperparameters, such as data augmentation and optimizers (and their respective learning rates), were the same as in the case of CNN-REG.

After enhancing the originally proposed MLSTM-CNN, the best performing parameters for *MSTM-CNN-ENH* were: data augmentation *row-wise*, optimizer *ADAM* with a learning rate set to $\alpha = 0.005$, and scaling factor $\kappa = 5$. On the other hand, the best performing parameters for *MLSTM-CNN-ORG* were: data augmentation *batch-wise*, and optimizer *SGD* with learning rate $\alpha = 0.005$.

2.3.3. Sliding puzzle network: original and enhanced

The sliding puzzle neural network (SP-NN) proposed in Mak and Düz (2019) has a pretty neat motivation. This model aims to shuffle random patches of the input data in a manner that resemble a sliding puzzle. In a sliding puzzle, although the image is shuffled, the content of the

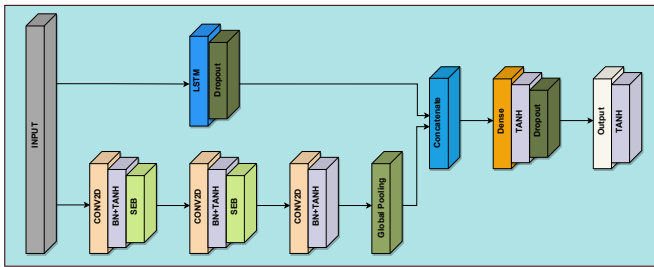


Figure 9: The architecture of the multivariate LSTM-CNN (MLSTM-CNN).

image can still be seen. This idea led to the construction of the NN, which topology can be seen in Figure 10. The SP-NN is designed to remove the positional dependency between samples completely. To achieve this, the average, max, and min pooling are performed for each feature map of the second convolution layer. As the original authors state: the result of encoding is purely based on initial convolutions.

We have built two versions of SP-NN: the original one that resembles the model proposed by its authors (*SP-NN-ORG*) and an enhanced one (*SP-NN-ENH*) where we increased the width of *SP-NN-ORG* by a factor κ . Therefore *SP-NN-ORG* had the following hyperparameters: the first convolution layer had 64 filters with kernel size 1×25 , the second convolution layer had 128 filters with kernel size 3×1 , dense layer consisted of 30 neurons, SEB block had shrink ratio of 16. Since the authors did not mention the kernel sizes of the max, average, and min pooling layers, we have tested the following kernel sizes: 1×1 , 3×3 , 5×5 , 7×7 , and 10×10 for both versions. Furthermore, we have trained SP-NN without any data augmentation, as well as with "row-wise" and "batch-wise" augmentation. The tested optimizers and respective learning rates were the same as for CNN-REG and MLSTM-CNN.

For the *SP-NN-ENH* we have scaled a number of filters and neurons by multiplying them with factor $\kappa = 10$. Optimizer for *SP-NN-ENH* was adam with $\alpha = 0.00005$. The optimizer for the original version was SGD with $\alpha = 0.005$.

We believe that we have enhanced all NNs in a manner that does not violets the original author's reasons and motivation behind NN design. Also, wherever we had doubts about parameters' values (when these were not specified in the original work), we tested different parameter values and took the best-performing one.

2.3.4. Attention-based neural network (AT-NN)

Many state-of-the-art algorithms in computer vision, natural language processing (NLP), or even augmented data generation rely on attention modules Galassi, Lippi and Torroni (2021); Zhang, Goodfellow, Metaxas and Odena (2019); Woo, Park, Lee and Kweon (2018). The attention module, including the self-attention module, has been introduced in paper Vaswani et al. (2017), which claims that "Attention is all you need." The intuition behind the attention module comes from NLP, where the urge to capture

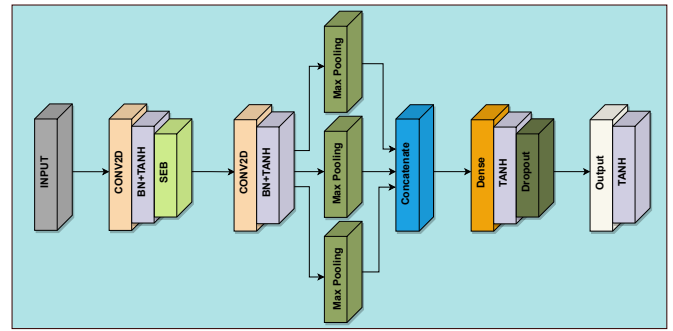


Figure 10: The architecture of the sliding puzzle neural network (SP-NN).

relations between words far away from each other in a sentence/text was necessary. Namely, one word can contain crucial information that, in combination with another word (for instance, a subject in the sentence), would completely change the sentence's meaning. However, this information can be spread along the whole text, so the NNs that are based on memory cells (LSTM Yu, Si, Hu and Zhang (2019)) or windows (CNN) would be incapable of capturing it.

We believe that the time-series signals describing the ship's motion have also scattered information that needs to be grouped. The proposed model AT-NN can seize the interaction and correlation between different parts of the input signals by utilizing the self-attention module. Thus, the model can create new informative features essential for sea state estimation, which simple convolution operations can not obtain.

The architecture of the proposed AT-NN is depicted in Figure 11. At the beginning of the NN, the heave, pitch, and yaw signals are merged into one embedded signal by performing 2D convolution with kernel size 3×125 . Since we utilized 128 kernels in this operation, NN operates on 128 embedded signals instead of three original ones. Besides merging three signals into one, the convolution operation also resulted in 1,377 overlapping window positions over the original signals. Each window captured 125 samples of the input signals. These overlapping window positions are equivalent to the "tokens" in the NLP models. Established practice in NLP recommends that each token have its position in sentence/signal encoded because the inter-token positions may be relevant information Jaderberg, Simonyan, Zisserman and kavukcuoglu (2015). We have followed this practice and utilized the sin and cosine encoding as proposed in Vaswani et al. (2017).

After merging and tokenizing the input signals, the proposed AT-NN utilizes two self-attention blocks. As depicted in Figure 11, each self-attention block consists of two multi-head attention (MHA) layers followed by a normalization layer. The attention mechanism is given by the equation 7:

$$attention(Q, K, V) = softmax\left(\frac{QK^T}{\sqrt{d_k}}\right)V \quad (7)$$

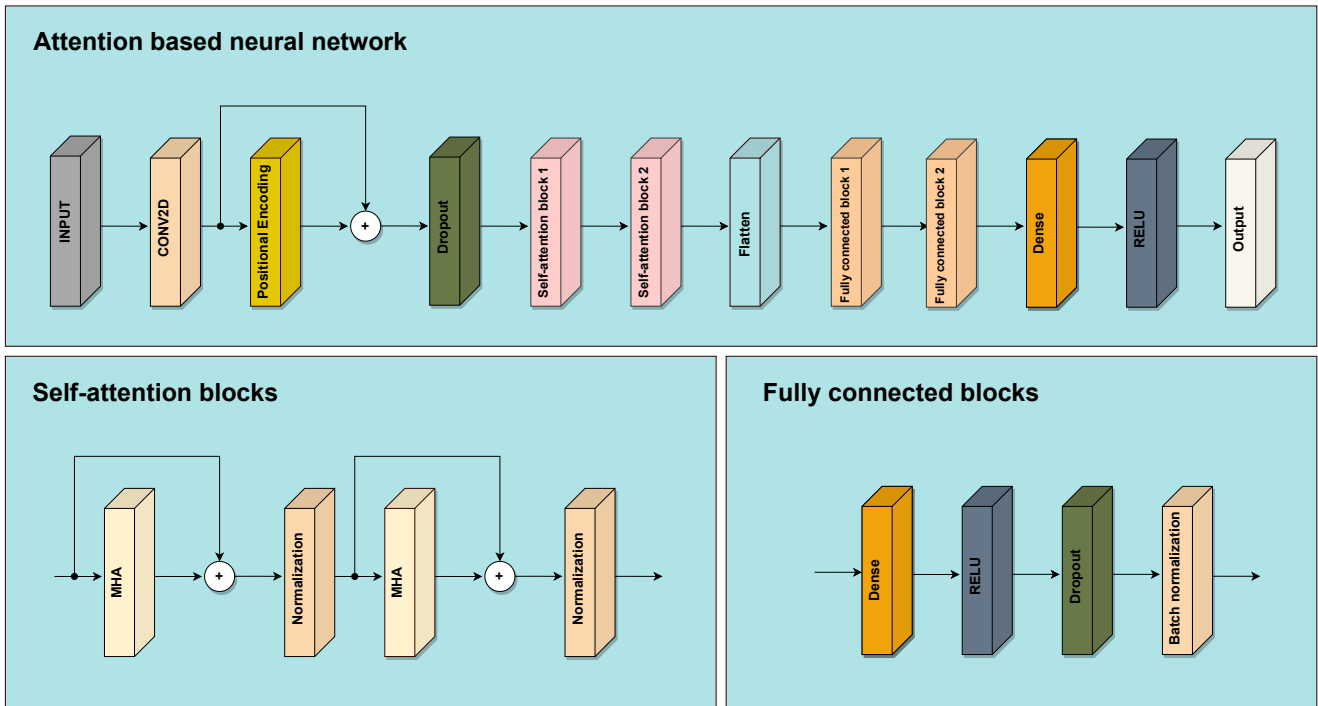


Figure 11: The architecture of the attention based neural network (AT-NN).

where Q , K , and V represent query, key, and value matrices, respectively, with their weights included (W_q, W_k, W_v) . In our case, we used self-attention where Q , K , and V were all equal to the layer's input. Generally speaking, the self-attention mechanism seeks relations between the tokens in the same input signal, not between the observed input signal and another different signal. Parameter d_k is a scaling factor equal to the length of the input embedding (in our case, 1,377).

On the other hand, the MHA is a mechanism that applies the self-attention mechanism several times in parallel, learning different relations between tokens simultaneously. The MHA is given by the equation 8:

$$\begin{aligned} \text{multihead}(Q, K, V) &= \text{concat}(\text{head}_1, \dots, \text{head}_i)W^l \\ \text{head}_i &= \text{attention}(Q, K, V) \end{aligned} \quad (8)$$

Each of $i = 2$ heads uses its own weights W_q^i, W_k^i , and W_v^i , which consequently means that each head learns different relations between tokens. Finally, heads' outputs are concatenated into one embedding. Embedding is scaled to match the original input "embedding" size by performing a simple linear projection utilizing weights W^l . Furthermore, the output of MHA is added to its input. After the addition is performed, the final summed output of the MHA is normalized. Normalization is done by subtracting the embedding mean value from the embedding values and dividing it by their standard deviation Garbin, Zhu and Marques (2020). The described mechanism is repeated two times in one self-attention block, as depicted in Figure 11. AT-NN model was built from two consecutive self-attention blocks.

The final embedding calculated by the second MHA ($batch_{size} \times 128 \times 1,377$) is flattened into $batch_{size}$ number of 1D vectors with a length of 176,256. This is important because the next part of the proposed AT-NN consists of fully-connected (dense) layers. As depicted in Figure 11, the AT-NN consists of three dense layers. The first dense layer has 128 neurons and is followed by the RELU activation function, dropout layer, and batch normalization layer Agarap (2018); Santurkar, Tsipras, Ilyas and Madry (2018). The second dense layer had 64 neurons, followed by the RELU activation function, dropout layer, and batch normalization layer. The last dense layer had only three neurons. Each of the three neurons represents outputs of the AT-NN: H_s , T_z , and β , respectively. The final output is one more time activated by the RELU activation function to avoid small negative number predictions. It is necessary to mention that all dropout layers (everywhere in AT-NN) had dropout probability set to 0.1 Baldi and Sadowski (2013).

Speaking of dropout layers, besides regularization purposes, they play a key role in the uncertainty estimation of the NN's decision. Uncertainty estimation raises the trustworthiness of models' predictions. The dropout method's uncertainty estimation is based on Monte-Carlo sampling of different variations of the original NN during the prediction. As proved in Gal and Ghahramani (2016), the sampled NNs can be treated as approximate Bayesian inference in deep Gaussian processes. To the best of our knowledge, our model is the first to introduce uncertainty estimation to the DL models for sea state estimation.

All parameter selection is made after a computationally heavy best-parameter combination search. That being said,

Table 2

An overview of the best performing hyperparameters for each model.

Model	DATA_AUG	OPTIMIZER	LR	SCALE	MAXPOOL	BLOCKS	NUM HEADS	EMB SIZE	NUM EMB	HEADS NEURONS
CNN-REG-ORG	Row-wise	SGD	0,005	3	1	/	/	/	/	/
MSTM-CNN-ORG	Batch-wise	SGD	0,005	1	/	/	/	/	/	/
SP-NN-ORG	Batch-wise	SGD	0,005	5	1	/	/	/	/	/
CNN-REG-ENH	Row-wise	ADAM	0,0005	10	5	/	/	/	/	/
MLSTM-CNN-ENH	Row-wise	ADAM	0,005	5	/	/	/	/	/	/
SP-NN-ENH	Batch-wise	ADAM	0,00005	10	5	/	/	/	/	/
AT-NN	Batch-wise	ADAM	0,0005	/	/	2	2	125	128	128,64,3

we have considered the following values as the candidates for chosen hyperparameters:

- number of MHA blocks: 2, 4, 8,
- number of heads in each MHA block: 2, 4, 8,
- token size: 125, 250, 500,
- number of embeddings: 32, 64, 128, 256,
- number of neurons in fully connected layers consecutively: (128, 64, 3), (256, 128, 3), (512, 256, 3), and (1, 024, 512, 3),
- Tested optimizers were *ADAM* and *SGD* both with learning rates $\alpha = 5 \cdot 10^{-3}, 5 \cdot 10^{-4}, 5 \cdot 10^{-5}$ Kingma and Ba (2014); Bottou (2012),
- Data augmentation: *row-wise* and *batch-wise*.

The model was trained with $batch_{size}$ set to 32 for 250 epochs with early stopping if there was no change in loss function on the validation data set for 10 epochs. The best model consisted of 2 MHA blocks with 2 heads each, a token size of 125, and the number of embeddings set to 128. The number of neurons in dense layers was (128, 64, 3) respectively, while the optimizer was ADAM with a learning rate set to 5×10^{-4} .

2.4. Hyperparameter overview and training setup

The overview of the best-performing hyperparameters for each model is given in Table 2. Since we trained a large number of models, the best performance (top 25), conducted with different hyperparameters, was achieved by those that used some kind of data augmentation. However, there is no evident distinction between the two types of augmentation (batch-wise and row-wise) in terms of the produced results.

The loss function was mean squared error (MSE) James and Stein (1992). The training process mentioned in section 2.3.4 was the same for all models: batch size was always set to 32, with early stopping after there was no improvement on validation loss of 10 epochs. The constraint that the models are training for 250 epochs was never fulfilled because all models converged after the 100 to 150 epoch.

Next, we provide the achieved results for all tested models and elaborate on their efficiency, advantages, and limitations.

3. Results and discussion

3.1. NN models performance

Evaluation of model performances is done separately for each sea state parameter: H_s , T_z , and β . We have calculated two metrics: MSE and mean absolute error (MAE) Chai and Draxler (2014) on both validation and test sets. The motivation behind utilizing these metrics as evaluation is in their nature. Namely, when training NNs, it is necessary to focus the models on the most troublesome samples. This behaviour can be achieved through MSE because it makes small errors (correct predictions) even smaller. At the same time, it increases the influence of errors in samples that the model did not predict correctly (or was the furthest from the correct prediction). On the other hand, we have also utilized MAE, which may be considered a reliable and realistic metric for the real-life scenario of sea state estimation.

Tables 3 and 4 present model results for each estimated parameter on validation and test set respectively. As can be seen, columns named MSE and MAE represent the average MSE and average MAE of the three estimated sea parameters (showing the general score of the models over all three estimated sea state parameters).

By inspecting the difference of respective scores between the validation and test set (Tables 3 and 4), it can be noticed that the models' performances have small deviations. This proves that models were appropriately trained and that early stopping indeed stops the models from over-fitting. Further investigation of the results shows a noticeable difference in performance between the enhanced group of models (including AT-NN) and the original models proposed in Mak and Düz (2019). This reflects all estimated sea state parameters and general scores. The difference between original and enhanced models (including the proposed model AT-NN) is quite large: by a factor 5×. For instance MSE *CNN-REG-ORG* is 0.0035, while the MSE of *CNN-REG-ENH* is 0.00059. The same applies to all other models on both validation and test sets. To support our claims and make results easier to follow, in Figure 12 we present box-plot diagrams of MSE and MAE on the test set. From the provided box plots, it is evident that we have successfully enhanced the original models.

Since the dataset in the paper Mak and Düz (2019) was not publicly available, we could not apply our method to it, and we had to re-implemented all of the models. By comparing their loss values results on the validation set

Table 3

 Models results of estimated parameters on validation dataset ($\times 10^{-3}$).

Model	MSE			MAE			MSE	MAE
	H_s	T_z	β	H_s	T_z	β		
CNN-REG-ORG	5,28544	3,889443	1,252465	57,042372	50,812191	26,702811	3,475783	37,110115
MLSTM-CNN-ORG	4,941625	4,194312	1,113016	56,162481	53,026415	25,387024	3,416318	37,535071
SP-NN-ORG	5,225949	4,765217	1,413309	57,096877	54,959986	26,934951	3,801492	38,619452
CNN-REG-ENH	0,93894	0,478358	0,210208	23,320904	16,435646	11,417285	0,542502	13,433017
MLSTM-CNN-ENH	1,259706	0,604518	0,29818	26,476073	19,144859	13,941651	0,720801	15,447244
SP-NN-ENH	1,289881	0,75156	0,169424	26,581532	19,68622	9,921086	0,736955	15,668236
AT-NN	0,802887	0,372965	0,115358	20,823295	13,835668	7,599803	0,430403	11,696455

Table 4

 Models results of estimated parameters on test dataset ($\times 10^{-3}$).

Model	MSE			MAE			MSE	MAE
	H_s	T_z	β	H_s	T_z	β		
CNN-REG-ORG	5,039482	3,939628	1,619829	55,412124	50,962495	28,444887	3,53298	36,635866
MLSTM-CNN-ORG	4,886629	4,118302	1,555991	55,245936	52,170407	28,296627	3,520307	36,978883
SP-NN-ORG	5,262113	4,662741	1,902819	58,077689	53,857223	28,712736	3,942557	38,625823
CNN-REG-ENH	0,981791	0,561467	0,231101	24,165625	17,323201	11,694066	0,591453	14,02676
MLSTM-CNN-ENH	1,345254	0,691574	0,290011	26,954267	20,597859	13,599609	0,775613	16,109246
SP-NN-ENH	1,25686	0,861854	0,216848	26,767925	21,339719	10,730237	0,77852	16,295388
AT-NN	0,851608	0,404057	0,114521	21,122448	13,955757	7,485123	0,456728	11,844978

(MSE = 0.05), we can conclude that produced results using the original models are improved. In our study, instead of 6-DOF motions, only 3-DOF was used as input parameters. Accordingly, we successfully demonstrated that original models achieve the same or better results with reduced input data. This is also, besides estimation accuracy, one of the advantages of here proposed approach.

Next, we point out the fact that our proposed model achieved the best results among all tested models. In both tables 3 and 4) the best results on each estimated parameter are bolded. Therefore, the best overall MSE on the test set was $MSE(AT-NN) = 0.00046$ for the proposed model with its $MAE(AT-NN) = 0.012$. The runner-up model was *CNN-REG-ENH* model with $MSE = 0.00059$ and $MAE = 0.014$. Since the error was already small ($< 10^{-3}$) achieved by existing models, the improvement made by the proposed model AT-NN was impactful. In other words, the AT-NN improved the MSE by 22.778% and MAE by 15.554% over the best-performing enhanced model.

According to the results in Table 4, one can see that the proposed AT-NN model achieves up to 94% improvement of MSE, and up to 70% improvement of MAE, compared to the original models (denoted by CNN-REG-ORG, MLSTM-CNN-ORG, and SP-NN-ORG). Also, the enhanced models performed better than the above-mentioned original models, so a valid comparison is a comparison between the proposed model and these enhanced models. The enhanced SP-NN model provided the best estimation of the angle β if we observe MSE and MAE for this parameter. However, the AT-NN model can achieve even more pronounced improvement. Namely, the MSE value is improved by 47% and MAE by 30% compared to SP-NN-ENH. This improvement is also

the largest in terms of estimation of angle β , achieved with the AT-NN model.

When analyzing the estimation results for H_s and T_z , CNN-REG-ENH distinguished out among the enhanced models with the best results. Again, AT-NN improves the results of the best-enhanced model. The proposed model improve MSE 13% and MAE 13% for H_s , MSE 28% and MAE 19% for T_z parameter in comparison to the best performing enhanced models. In comparison to the original models, the improvement is even more significant in all the observed parameters. Observing the performance of the AT-NN model, the estimation of the period T_z and the angle β achieves the most favorable advancements compared to the estimation of the parameter H_s .

To increase the trustworthiness of the proposed model, we have enabled uncertainty estimation as an additional feature.

3.2. Uncertainty estimation

As mentioned in subsection 2.3.4, adding dropout layers to the "head" part of the AT-NN model enabled the utilization of Monte-Carlo sampling. By utilizing Monte-Carlo dropout sampling, we simulated the Gaussian process and, therefore, obtained model prediction uncertainty for each estimated sea state parameters Gal and Ghahramani (2016). The process is quite simple in bolt and nuts: for the same input time-series signals, we run predictions of the AT-NN 256 times, on every prediction dropping random neurons. By dropping random neurons, we obtain a new version of the original NN that gives predictions slightly different from other "sampled" networks. By calculating the mean value μ standard deviation σ of all predictions, we can

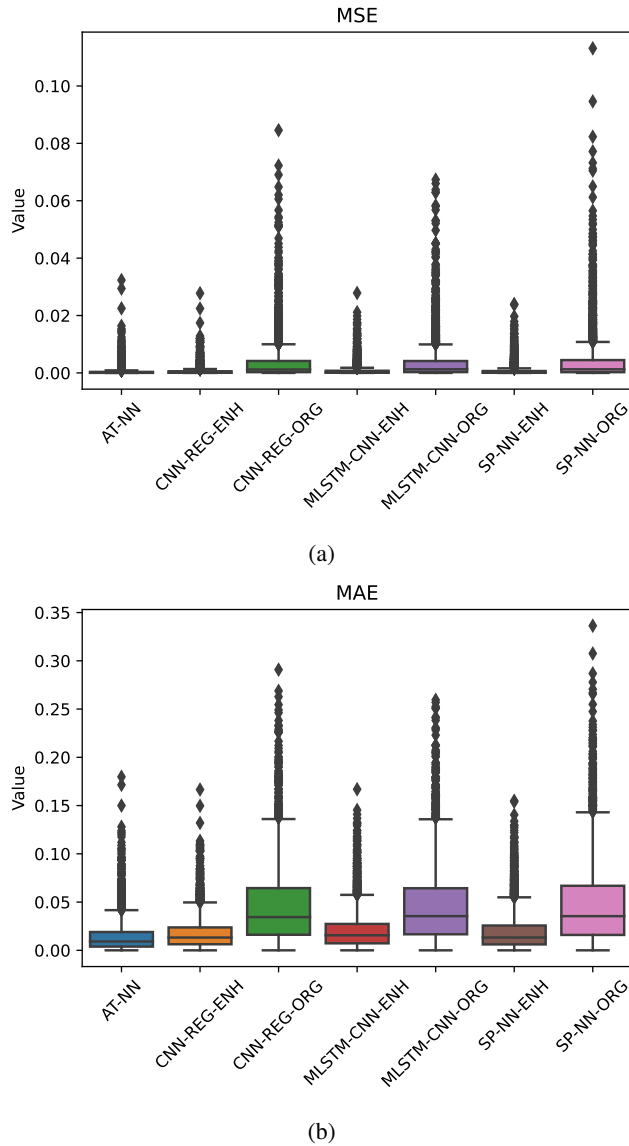


Figure 12: Box-plot diagrams on the test set with two measures: a) MSE and b) MAE.

calculate a Gaussian curve that estimates the uncertainty of the model decision. Accompanying uncertainty estimation, we also have the actual prediction of the model generated without dropping any of the neurons.

To increase explainability and provide additional information, we have extended the output of Monte-Carlo dropout sampling by involving statistical measurement. Although quite simple in its nature, statistical measurement involved counting how many correct measurements of the test set fell into Gaussian curves estimated by Monte-Carlo dropout sampling with different values of σ (μ was fixated). The different values of σ were calculated by multiplying sigma with $n \in [1, 2, 3, 4, 5]$ resulting in wider Gaussian curves. Thus, following one's expectation, wider Gaussian curves would also encompass a bigger number of correct measurements of the sea state. Therefore for $n = 1$, the Gaussian curve with $\sigma_{\text{scaled}} = 1 \times \sigma$ contained 387 correct predictions while

896 predictions/samples were outside the range. This leads us to 30% certainty in total (387/1283) for this quite narrow, Gaussian curve. On the other hand, a much wider Gaussian curve with $\sigma_{\text{scaled}} = 5 \times \sigma$ contained 1246 predictions from 1283 samples in test set which lead us to the certainty of 97%. The validation dataset had similar performance related to σ values and the number of contained samples, so the integrity of the estimation was not impaired. The graphical example of the final AT-NN output is given in Figure 13. It can be seen that the blue line represents the true value for the given input signals, and the black line represents the prediction of the AT-NN without dropping any neurons. In contrast, Gaussian curves represent different "intervals"/"areas" of probability that correct measurements lie within. We believe that this novel process of estimating and interpreting the NN's output raises the trustworthiness of the proposed model. Also, besides having only one number, as a result, the user of the proposed model, if having doubts in model estimation, now has confidence levels provided by different Gaussian curves. We believe that uncertainty estimation tailored in the previously described way can be crucial information in various practical scenarios.

3.3. Summary of contributions and novelty

Let us conclude our study by clearly pointing out the achievements and novelty introduced in this manuscript, summarized as follows:

- We have retrained the existing state-of-the-art models proposed in Mak and Düz (2019) and enhanced them by increasing their width. The enhanced models performed better than the originally proposed models.
- We have proven that it is possible to obtain similar or better results by only 3-DOF ship motion responses instead of using 6-DOF ship motion responses (sea state parameters' estimation improved by 23% in terms of MSE and by 16% in terms of MAE).
- As guidelines for model training, we have dug into data augmentation methods based on shuffling input signal slices. The investigation concludes that all tested models achieve better results with shuffled input signals' slices.
- We have proposed a novel AT-NN model that achieved the best results among all tested models for each estimated sea state parameter. To the best of our knowledge, this is the first time the AT-NN to be implemented for sea state estimation.
- Furthermore, in this manuscript, we have proposed a novel way of interpreting the uncertainty estimation of NN outputs based on the Monte-Carlo dropout method. The way we interpret the uncertainty of the model's predictions would raise the model's trustworthiness even if his initial prediction achieved a negligible error rate. Also, this is the first time for the

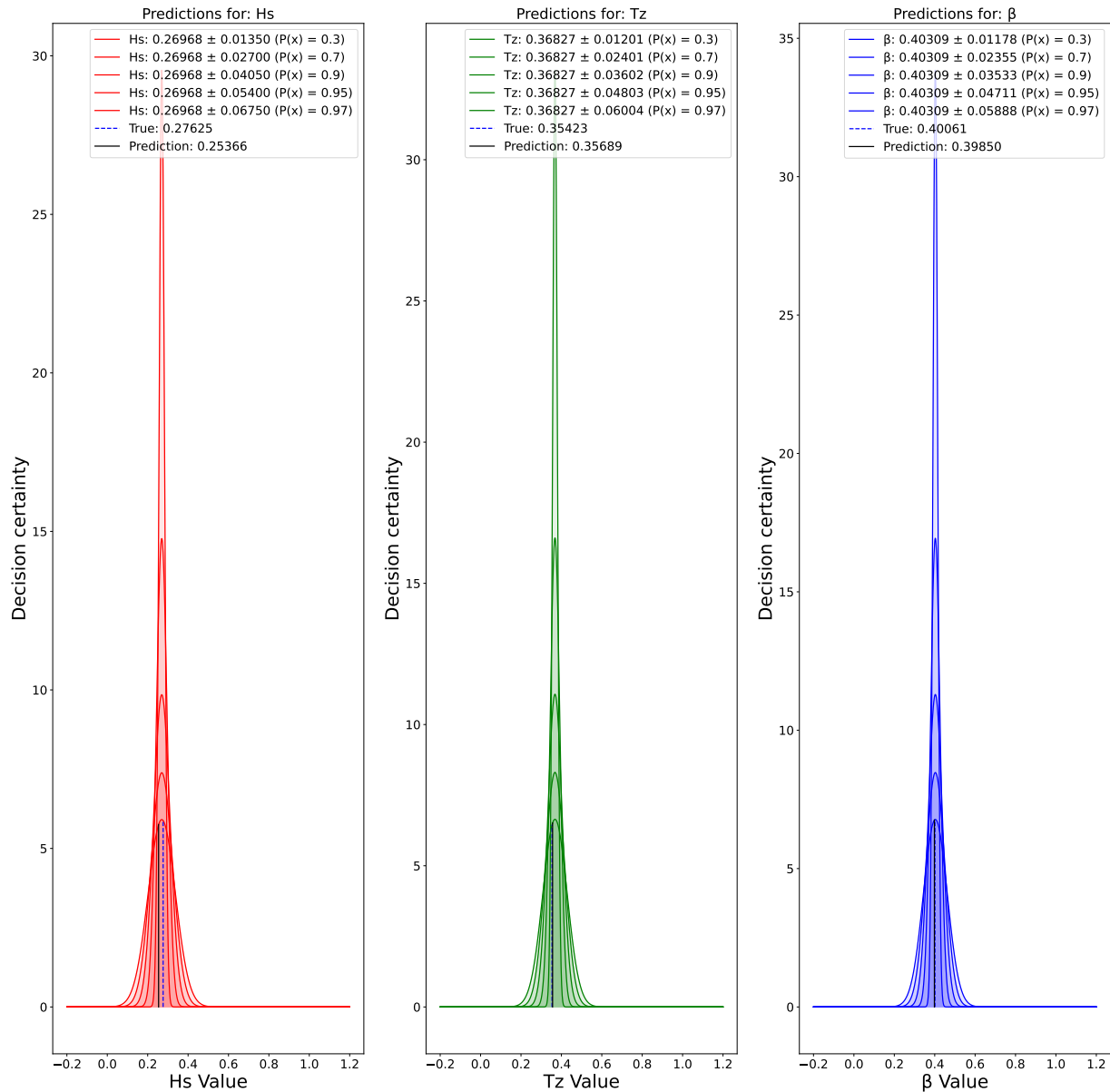


Figure 13: Uncertainty estimation of NN outputs H_s , T_z and β based on Monte-Carlo dropout.

uncertainty estimation of the DL models in the sea state estimation, according to the extensive literature review.

4. Conclusion

The paper presents a novel attention-based DL model for estimating important sea state characteristics. By evaluating the performance for each sea state parameter, we confirm that the AT-NN model is fine-tuned and suitable for estimating key sea state parameters. The improvement made by the proposed AT-NN model proved significant as MSE was reduced by about 23% and MAE by about 16%, compared to the best versions of the original, formerly proposed state-of-the-art models. Despite using 3-DOF input motion data, the

proposed model achieved the best results among all tested, original and enhanced models for each estimated sea state parameter. In practical applications, entire wave directional spectrum estimation is of great importance. Therefore, future work directions may include information about wave directionality in numerical simulations that can extend the application of the DL model to short-crested waves and combined wind and swell sea spectrums.

Declaration of competing interest

The authors declare no conflict of interest.

CRedit authorship contribution statement

Denis Selimović: Conceptualization, Methodology, Software, Validation, Investigation, Data Curation, Writing – Original Draft Preparation, Visualization. **Franko Hrzić:** Conceptualization, Methodology, Software, Validation, Investigation, Data Curation, Writing – Original Draft Preparation, Visualization. **Jasna Prpić-Oršić:** Conceptualization, Methodology, Validation, Formal Analysis, Resources, Data Curation, Writing – Review & Editing, Supervision, Project Administration, Funding Acquisition. **Jonatan Lerga:** Conceptualization, Methodology, Validation, Formal Analysis, Investigation, Resources, Writing – Original Draft Preparation, Writing – Review & Editing, Supervision, Project Administration, Funding Acquisition.

Funding

This work was fully supported by the Croatian Science Foundation under the project IP-2018-01-3739, EU Horizon 2020 project "INNO2MARE" under the number 101087348, IRI2 project "AbsistemDCiCloud" (KK.01.2.1.02.0179), University of Rijeka projects uniri-tehnic-18-17 and uniri-tehnic-18-15 and the European COST project CA17137.

References

- Agarap, A.F., 2018. Deep learning using rectified linear units (relu). CoRR abs/1803.08375. URL: <http://arxiv.org/abs/1803.08375>, arXiv:1803.08375.
- Baldi, P., Sadowski, P.J., 2013. Understanding dropout, in: Burges, C., Bottou, L., Welling, M., Ghahramani, Z., Weinberger, K. (Eds.), *Advances in Neural Information Processing Systems*, Curran Associates, Inc. URL: <https://proceedings.neurips.cc/paper/2013/file/71f6278d140af599e06ad9bf1ba03cb0-Paper.pdf>.
- Bottou, L., 2012. *Stochastic Gradient Descent Tricks*. Springer Berlin Heidelberg, Berlin, Heidelberg. pp. 421–436. URL: https://doi.org/10.1007/978-3-642-35289-8_25, doi:10.1007/978-3-642-35289-8_25.
- Chai, T., Draxler, R.R., 2014. Root mean square error (rmse) or mean absolute error (mae)? – arguments against avoiding rmse in the literature. *Geoscientific Model Development* 7, 1247–1250. URL: <https://gmd.copernicus.org/articles/7/1247/2014/>, doi:10.5194/gmd-7-1247-2014.
- Cheng, X., Li, G., Ellefsen, A., Chen, S., Hildre, H., Zhang, H., 2020a. A novel densely connected convolutional neural network for sea state estimation using ship motion data. *IEEE Transactions on Instrumentation and Measurement* PP, 1–1. doi:10.1109/TIM.2020.2967115.
- Cheng, X., Li, G., Skulstad, R., Chen, S., Hildre, H., Zhang, H., 2019. Modeling and analysis of motion data from dynamically positioned vessels for sea state estimation, pp. 6644–6650. doi:10.1109/ICRA.2019.8794069.
- Cheng, X., Li, G., Skulstad, R., Zhang, H., Chen, S., 2020b. Spectralseanet: Spectrogram and convolutional network-based sea state estimation, in: *IECON 2020 The 46th Annual Conference of the IEEE Industrial Electronics Society*, pp. 5069–5074. doi:10.1109/IECON43393.2020.9254890.
- Denis, M., Pierson, W., 1953. *On the Motions of Ships in Confused Seas*. Defense Technical Information Center. URL: <https://books.google.hr/books?id=38i6oAEACAAJ>.
- DNV-GL, 2018. *Class guideline: Wave loads*. DNVGL-CG-0130 , 84Edition January.
- Duz, B., Mak, B., Hageman, R., Grasso, N., 2019. Real time estimation of local wave characteristics from ship motions using artificial neural networks.
- Faltinsen, O.M., 1990. *Sea Loads on Ships and Offshore Structures*. Cambridge University Press, The Edinburgh Building, Cambridge CB2 2RU, UK.
- Gal, Y., Ghahramani, Z., 2016. Dropout as a bayesian approximation: Representing model uncertainty in deep learning, in: Balcan, M.F., Weinberger, K.Q. (Eds.), *Proceedings of The 33rd International Conference on Machine Learning*, PMLR, New York, New York, USA. pp. 1050–1059. URL: <https://proceedings.mlr.press/v48/gal16.html>.
- Galassi, A., Lippi, M., Torroni, P., 2021. Attention in natural language processing. *IEEE Transactions on Neural Networks and Learning Systems* 32, 4291–4308. doi:10.1109/TNNLS.2020.3019893.
- Garbin, C., Zhu, X., Marques, O., 2020. Dropout vs. batch normalization: an empirical study of their impact to deep learning. *Multimedia Tools and Applications* 79, 12777–12815. URL: <https://doi.org/10.1007/s11042-019-08453-9>, doi:10.1007/s11042-019-08453-9.
- Hinostroza, M., Guedes Soares, C., 2016. Parametric estimation of the directional wave spectrum from ship motions. *The International Journal of Maritime Engineering* 158, A121–A130. doi:10.3940/rina.2016.a2.356.
- Hochreiter, S., Schmidhuber, J., 1997. Long short-term memory. *Neural Computation* 9, 1735–1780. doi:10.1162/neco.1997.9.8.1735.
- Hu, J., Shen, L., Sun, G., 2018. Squeeze-and-excitation networks, in: *Proceedings of the IEEE Conference on Computer Vision and Pattern Recognition (CVPR)*.
- ITTC (Ed.), 1969. *Proceedings of the 12th International Towing Tank Conference*. volume 1, ITTC. URL: <https://www.ittc.info/media/2745/index.pdf>.
- Jaderberg, M., Simonyan, K., Zisserman, A., kavukcuoglu, k., 2015. Spatial transformer networks, in: Cortes, C., Lawrence, N., Lee, D., Sugiyama, M., Garnett, R. (Eds.), *Advances in Neural Information Processing Systems*, Curran Associates, Inc. URL: <https://proceedings.neurips.cc/paper/2015/file/33ceb07bf4eeb3da587e268d663aba1a-Paper.pdf>.
- James, W., Stein, C., 1992. *Estimation with Quadratic Loss*. Springer New York, New York, NY. pp. 443–460. URL: https://doi.org/10.1007/978-1-4612-0919-5_30, doi:10.1007/978-1-4612-0919-5_30.
- Kingma, D.P., Ba, J., 2014. Adam: A method for stochastic optimization. URL: <https://arxiv.org/abs/1412.6980>, doi:10.48550/ARXIV.1412.6980.
- Mak, B., Düz, B., 2019. Ship As a Wave Buoy: Estimating Relative Wave Direction From In-Service Ship Motion Measurements Using Machine Learning. URL: <https://doi.org/10.1115/OMAE2019-96201>, doi:10.1115/OMAE2019-96201.
- Mittendorf, M., Nielsen, U., Bingham, H., 2022. The prediction of sea state parameters by deep learning techniques using ship motion data.
- Montazeri, N., Nielsen, U.D., Juncher Jensen, J., 2016. Estimation of wind sea and swell using shipboard measurements – a refined parametric modelling approach. *Applied Ocean Research* 54, 73–86. URL: <https://www.sciencedirect.com/science/article/pii/S0141118715001388>, doi:https://doi.org/10.1016/j.apor.2015.11.004.
- Nielsen, U., Bjerregård, M., Galeazzi, R., Fossen, T., 2015. New concepts for shipboard sea state estimation. doi:10.23919/OCEANS.2015.7404386.
- Nielsen, U.D., 2006. Estimations of on-site directional wave spectra from measured ship responses. *Marine Structures* 19, 33–69. URL: <https://www.sciencedirect.com/science/article/pii/S0951833906000529>, doi:https://doi.org/10.1016/j.marstruc.2006.06.001.
- Nielsen, U.D., 2017. A concise account of techniques available for shipboard sea state estimation. *Ocean Engineering* 129, 352–362. URL: <https://www.sciencedirect.com/science/article/pii/S0029801816305388>, doi:https://doi.org/10.1016/j.oceaneng.2016.11.035.
- Nielsen, U.D., Galeazzi, R., Brodtkorb, A.H., 2016. Evaluation of shipboard wave estimation techniques through model-scale experiments, in: *OCEANS 2016 - Shanghai*, pp. 1–8. doi:10.1109/OCEANSAP.2016.7485701.
- Pascoal, R., Guedes Soares, C., 2009. Kalman filtering of vessel motions for ocean wave directional spectrum estimation. *Ocean Engineering* 36, 477–488. URL: <https://www.sciencedirect.com/science/article/pii/S0029801809000183>, doi:https://doi.org/10.1016/j.oceaneng.2009.01.013.
- Pascoal, R., Perera, L., Guedes Soares, C., 2017. Estimation of directional sea spectra from ship motions in sea trials. *Ocean Engineering* 132, 126–137. URL: <https://www.sciencedirect.com/science/article/pii/S0029801817300288>, doi:https://doi.org/10.1016/j.oceaneng.2017.01.

020.

- Santurkar, S., Tsipras, D., Ilyas, A., Madry, A., 2018. How does batch normalization help optimization?, in: Bengio, S., Wallach, H., Larochelle, H., Grauman, K., Cesa-Bianchi, N., Garnett, R. (Eds.), *Advances in Neural Information Processing Systems*, Curran Associates, Inc. URL: <https://proceedings.neurips.cc/paper/2018/file/905056c1ac1dad141560467e0a99e1cf-Paper.pdf>.
- Scholcz, T., Mak, B., 2020. Ship as a wave buoy: Estimating full directional wave spectra from in-service ship motion measurements using deep learning. doi:10.1115/OMAE2020-18783.
- Selimović, D., Hržić, F., Prpić-Oršić, J., Lerga, J., 2022. Sea state estimation from ship motion responses using deep learning. public. URL: <https://github.com/fhrzic/DSelimovcProject.git>.
- Selimović, D., Lerga, J., Prpić-Oršić, J., Kenji, S., 2020. Improving the performance of dynamic ship positioning systems: A review of filtering and estimation techniques. *Journal of Marine Science and Engineering* 8. URL: <https://www.mdpi.com/2077-1312/8/4/234>, doi:10.3390/jmse8040234.
- Tannuri, E.A., Sparano, J.V., Simos, A.N., Da Cruz, J.J., 2003. Estimating directional wave spectrum based on stationary ship motion measurements. *Applied Ocean Research* 25, 243–261. URL: <https://www.sciencedirect.com/science/article/pii/S0141118704000070>, doi:<https://doi.org/10.1016/j.apor.2004.01.003>.
- Tu, F., Ge, S.S., Choo, Y.S., Hang, C.C., 2018. Sea state identification based on vessel motion response learning via multi-layer classifiers. *Ocean Engineering* 147, 318–332. URL: <https://www.sciencedirect.com/science/article/pii/S0029801817305188>, doi:<https://doi.org/10.1016/j.oceaneng.2017.08.047>.
- Vaswani, A., Shazeer, N., Parmar, N., Uszkoreit, J., Jones, L., Gomez, A.N., Kaiser, L.u., Polosukhin, I., 2017. Attention is all you need, in: Guyon, I., Luxburg, U.V., Bengio, S., Wallach, H., Fergus, R., Vishwanathan, S., Garnett, R. (Eds.), *Advances in Neural Information Processing Systems*, Curran Associates, Inc. URL: <https://proceedings.neurips.cc/paper/2017/file/3f5ee243547dee91fbd053c1c4a845aa-Paper.pdf>.
- Woo, S., Park, J., Lee, J.Y., Kweon, I.S., 2018. Cbam: Convolutional block attention module, in: *Proceedings of the European Conference on Computer Vision (ECCV)*.
- Yu, Y., Si, X., Hu, C., Zhang, J., 2019. A Review of Recurrent Neural Networks: LSTM Cells and Network Architectures. *Neural Computation* 31, 1235–1270. URL: https://doi.org/10.1162/neco_a_01199, doi:10.1162/neco_a_01199.
- Zhang, H., Goodfellow, I., Metaxas, D., Odena, A., 2019. Self-attention generative adversarial networks, in: Chaudhuri, K., Salakhutdinov, R. (Eds.), *Proceedings of the 36th International Conference on Machine Learning*, PMLR. pp. 7354–7363. URL: <https://proceedings.mlr.press/v97/zhang19d.html>.